International Journal of Applied Earth Observation and Geoinformation 118 (2023) 103236

Contents lists available at ScienceDirect

International Journal of Applied Earth Observation and Geoinformation

journal homepage: www.elsevier.com/locate/jag

Contributions from experimental geostatistical analyses for solving the cloud-cover problem in remote sensing data

A. Tayebi, S. Kasmaeeyazdi, F. Tinti *, R. Bruno

Department of Civil, Chemical, Environmental and Materials Engineering, University of Bologna, via Terracini 28, 40121 Bologna, Italy

ARTICLE INFO

Keywords:
Geostatistical estimation
Sentinel-2 image
Cloud estimation

ABSTRACT

Nowadays, in many fields and applications, such as mining engineering, environmental monitoring, soil science, natural resources and environmental topics, the potential of Remote Sensing have been exploited. Large amount of data, easy and fast accessibility, and time–space availability are the reasons of attractiveness of satellite data in many fields of geosciences. However, satellite images face the problems due to presence of shadows and clouds, which is a general and real challenge since the surface features are masked. In many cases, a dense cloud cover simply prevents any detailed study of the target area through Earth Observation techniques. Geostatistics is a science field properly developed to estimate the unknown values in two-dimensional or three-dimensional space; therefore, it can be a potential approach to solve cloud-cover issues in Remote Sensing investigations. This work applies the geostatistical tools over a sentinel-2 satellite image targeting land cover in Emilia Romagna (Italy). The three main spectrum bands (RGB-values) with 10-m spatial resolution have been selected as target variables. The objective is to estimate pixel values within an area which is covered by clouds. The spatial variability of pixels with available land cover information have been studied through the use of variogram tools. Different estimation neighborhoods have been tested for application of the Kriging interpolation method, in order to estimate the RGB values below the cloud-covered area. The estimation has been performed, by controlling the properties of the estimator, the varying sizes and shapes of the neighborhood, the available number of RGB data used for estimation and the spatial distribution of pixels in the image. An image with close time period, without clouds, has been used to validate the results. Moreover, the estimation variance of RGB values for each pixel has been mapped. Results have shown the advantages and limitations of the proposed geostatistical method for the specific application of cloud-covered areas.

1. Introduction

Many applications exploit the support of data from Earth Observation for monitoring, mapping and land cover studies. As an example, a typical use of optical remote sensing data is related to maps creation and to evaluation of plant and vegetation growth (Rohden Prudente et al., 2020). Another widely used application belongs to the mining sector and is specific to identifying and mapping many environmental parameters (water, dust, vegetation health, acid mine drainage, etc.), which can be monitored using optical remote sensing data (Kayet et al., 2022; Pascucci et al., 2012; Swayze et al., 2000).

However, the monitoring of any selected feature (agricultural areas, mining fields, water resources, coastal studies, etc.) is strongly impacted by cloud cover. In many images, clouds cover small/large surface features and ground information. In all mentioned applications, the presence of the clouds reduces the availability of spatial–temporal data, and creates a gap or noise while analyzing the earth surface features (Wang, 2022). Hence, efforts to recover the missing information under clouds are desirable. Simulated and cloudy images are used and compared to validate the methodologies. According to literature, removing clouds processing methods are classified into three groups: multispectral complementation, multitemporal complementation, and spatial-complementation approaches (Meng et al., 2017). However, the spatial-complementation approaches are the main methods to reconstruct the missing areas covered by clouds. These approaches are based on image inpainting techniques that use the known ground information to fill the missing areas under the clouds. The best results of inpainting methods are obtained in small missing areas without textures.

Various algorithms can be used for inpainting of large areas and retaining the feature textures, such as patch-sparsity based inpainting as

* Corresponding author.
E-mail address: francesco.tinti@unibo.it (F. Tinti).

https://doi.org/10.1016/j.jag.2023.103236
Received 9 December 2022; Received in revised form 14 February 2023; Accepted 16 February 2023
Available online 26 February 2023

a method which can create sharp textures (Xu and Sun, 2010), Bandelet transform (Maalouf et al., 2009), or patch filling (Lorenzi et al., 2011) as other algorithms to implant the images.

A method proposed by Zhu is recovering the under clouds information by the neighborhood similar pixel interpolator (NSPI) approach (Zhu et al., 2012). Similarly, to produce imagery without clouds, Helmer and Ruefenacht have used regression trees and histogram matching (Helmer and Ruefenacht, 2005).

To reconstruct the spectral values of pixels for cloud covered areas, the closest spectral fit method (CSF) is adapted as a consistence approach (Meng et al., 2009) or the process of contextual multiple linear prediction (CMLP), which can be used to reconstruct the spectral values within an area which is covered by clouds (Melgani, 2006). In mentioned approaches, the image is reconstructed by the close data with the similar spectral characteristics, however, without considering the spatial and spectral correlations and continuities (Zhu et al., 2012).

Another method for pixel replacement is filling the missing ones by a similar value, obtained from adjacent parts of the image. To find the most appropriate pixel value, a global function based on pixel-offset and space–time Markov random fields (MRF) was tested. As a result of this, as an example, the land surface temperature was created from multi-temporal images (Cheng et al., 2014).

Recently, more advanced methods are used to fill the missing values covered by clouds. The machine learning algorithms (e.g. random forest algorithm) and deep learning (e.g. Datawig) (Wang, 2022) are those which are tested to fill the data covered by clouds in both multispectral and hyperspectral images (Wang and Wang, 2022). In another example, Deep learning is used to remove the cloud-cover using three temporal images (Jiang et al., 2022). In this work, authors have summarized methods used for cloud-removing since 2016, and classified them into: Multispectral-based methods, Inpainting-based methods and Multitemporal-based methods, which can be used in various applications (Jiang et al., 2022).

Based on the field of study and the features and textures of the target images, the most coherent methodology can be selected. As an example, in water bodies mapping, there is the need of an approach able to predict and model the abrupt changes (between land and water features). To tackle this challenge, some works have been done using a category-based method (Li et al., 2021). Here, authors suggested an approach to construct pixels under clouds for water bodies using "spatiotemporal dependence model". They proposed to use the same positions of the cloud-cover pixels from other images on other dates using the data distribution statistics and correlations (Li et al., 2021).

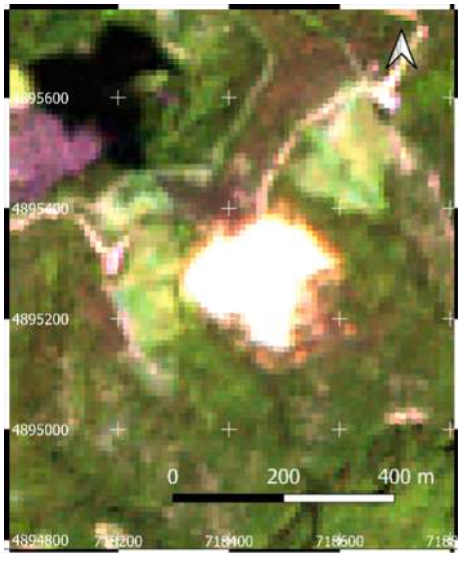

Fig. 1. Sentinel-2 image with thick cloud in the middle (44.177966, 11.732884), sensing 2019/06/23.

Another example has been focused on tropical areas. Hence, to map and classify the land cover under cloud-cover areas, authors presented the use of SAR data, because of their potential to penetrate clouds (Shrestha et al., 2019). Since authors focus on tropical areas, the surface roughness could be highly important and SAR intensity image could be a coherent solution. Specifically, authors have used the surface roughness with the terrain slope and elevation to solve the challenge of cloud cover (Shrestha et al., 2019).

Mining can be considered a field, with increasing application of remote sensing data (Van der Meer et al., 2014; Ibrahim et al., 2020; Ngom et al., 2022). However, with respect to previous examples, the target is usually a homogeneous zone with the same pattern (for example only naked soil, or only rocky land cover). On the other hand, the target is normally characterized by different mineral contents; for example, Al-bearing minerals (bauxite) present in fact multielement concentrations (Al, Fe, Ti, V…) (Kasmaeeyazdi et al., 2021). In such cases, in presence of cloud cover, smoother predicting methods should be tested instead of abrupt changes approaches, as for the previous examples. Therefore, in such cases a possible non-tested approach, to tackle the issue of cloud-removal, is using geostatistics (Matheron, 1971). This method is proposed since, similarly to an unknown area with few samples available, it is possible to predict (estimating or simulating) unknown points or blocks by using spatial variability models and geostatistical tools. In fact, the geostatistical estimation methods are particularly favorable to provide smooth prediction of unknown areas using available samples (Chilès and Delfiner, 1999). The reason lies in the original purpose of the geostatistical methodology, specifically developed to reduce at minimum the mining risk in the exploration phase.

In this work, as a novelty, the geostatistical prediction models are used to evaluate the possibility of filling pixels using spatial variability of image bands. The main objective of this study is testing the possibility of using Kriging approaches to estimate the missing pixels in remote sensing data, focusing on mining and adjacent areas. On such cases, there are less distinctive features (such as buildings, streets, etc.) but images are characterized by more homogenous areas (soil, rocks, naked lands with unique texture but various contents). Hence, sentinel-2 image on an area covered by grass and soil nearby a gypsum deposit in Italy is selected and preliminary spatial analysis is performed (see Section 2). Various parameters are tested to perform Kriging and to predict the missing values of the image. Final maps are created with the same spatial resolution of original image and comparisons among different results are shown (see Section 3). Results demonstrate the advantages and disadvantages of Kriging methods for filling the missing parts of an image (see Section 4). Finally, the methodology is tested for a larger area with more complex cloud cover (including one shadow and four clouds) in the discussion (see Section 4).

2. Materials and methods

In this work, to evaluate the possibility of predicting pixel values under clouds, for the first time, the Kriging interpolation is used (Armstrong, 1998). The main focus is the estimation of the RGB pixel values. To perform the estimation, various possibilities of selecting the input data are tested (as the neighborhoods), including various numbers of input data from different positions. In addition to the geostatistical estimation, the common simulation approach (used by other researchers mentioned in the introduction) is used for predicting the pixel values under clouds. In this approach, the similarity of pixel values in a "clean" image is considered. To fill the pixels under clouds, an additional image of the same location is selected (without cloud), with the same time period as the secondary image. Within the secondary image, a simple search is done to find the most similar values between the cloud-covered pixels (identified by the first image) and those pixels outside the cloud-covered area. So, those pixels outside the cloud-covered area with the

Table 1
Sentinel-2 band list (The European Space Agency, 2022).

Bands from Sentinel-2	Band description	Central Wavelength (μm)	Resolution (m)
Band 1	Coastal aerosol	0.443	60
Band 2	**Blue**	**0.490**	**10**
Band 3	**Green**	**0.560**	**10**
Band 4	**Red**	**0.665**	**10**
Band-5	Vegetation Red Edge	0.705	20
Band 6	Vegetation Red Edge	0.740	20
Band 7	Vegetation Red Edge	0.783	20
Band 8	NIR	0.842	10
Band 8A	Vegetation Red Edge	0.865	20
Band 9	Water vapour	0.945	60
Band 10	SWIR - Cirrus	1.375	60
Band 11	SWIR	1.610	20
Band 12	SWIR	2.190	20

most similar values are selected as the reference pixels. Coming back to the first image (with missing values), the reference pixels outside the cloud-covered area are used to select and fill each missing pixel value. Therefore, the results obtained by filling the pixels (simulated from the secondary image) are obtained and compared with the original image (covered by clouds). All approaches in this work are performed for three variables (three bands, RGB values) to get the possibility of making comparison between the images obtained from different approaches.

2.1. Case study

Based on the objective of this research, a sentinel-2 image is selected and a subset including cloud area is obtained for estimation. The main challenge is using the surrounded data to predict the under-cloud area within the image. The selected area is nearby a gypsum mine, including grassland, some sparse farms and soil covered area. The image is quite simple with small cloud, since the main objective is to test the possibility of using geostatistical estimation approaches to fill the cloud-covered pixels. The selected image is sensed on 2019/06/23 in the province of Ravenna, Italy (see Fig. 1), with the following coordinates:

Longitude: 11°43′57″ E.

Latitude: 44°10′40″ N.

Remotely sensed images are widely known and frequently used in many different scientific and engineering fields since they provide many information concerning the land surface (Patino and Duque, 2013). Sentinel-2 is a European mission, providing global acquisitions of high resolution and 13 spectral bands (The European Space Agency, 2022). In Table 1, the sentinel-2 bands are indicated.

The main focus is on the main three bands (RGB) to create a real colored image under the cloud. As it is shown in Fig. 1, there is a thick cloud in the middle of the image, covering more than 50,000 m^2 of the Earth's surface. For the three selected bands (RGB), the spatial resolution is 10 m (see Table 1).

2.2. Basic statistics

As the first step, statistical parameters for the selected variables, Band 2 (B2), Band 3 (B3) and Band 4 (B4) are studied. There are 8000 pixels, in total, including the cloud in the middle and the shadow of the cloud located on the top left of the image (see Fig. 1). In the following, the histogram and statistical parameters of B2 values are shown (Fig. 2).

As it is shown in the histogram of data, there are two extraordinary set of data with very high and very low values at both ends of the abscissa axis. These two classes of data are related to the shadow, with very low values close to 0, and to the cloud with high values within the distributions of three bands. Therefore, it is possible to highlight those pixels with cloud and shadow values in the image.

For estimation and statistical analysis of data, the pixels which have extraordinary values (cloud and shadow) are excluded. The following figures show the histogram of the three selected bands (RGB), excluding the shadow and the cloud (Figs. 3-5).

2.3. Spatial modelling

Geostatistical modeling, as proposed by Matheron, is an optimum method to predict the non-sample points, considering the spatial variability and randomness of the target variable (Matheron, 1971). For example, the geostatistical method of Kriging is an unbiased linear

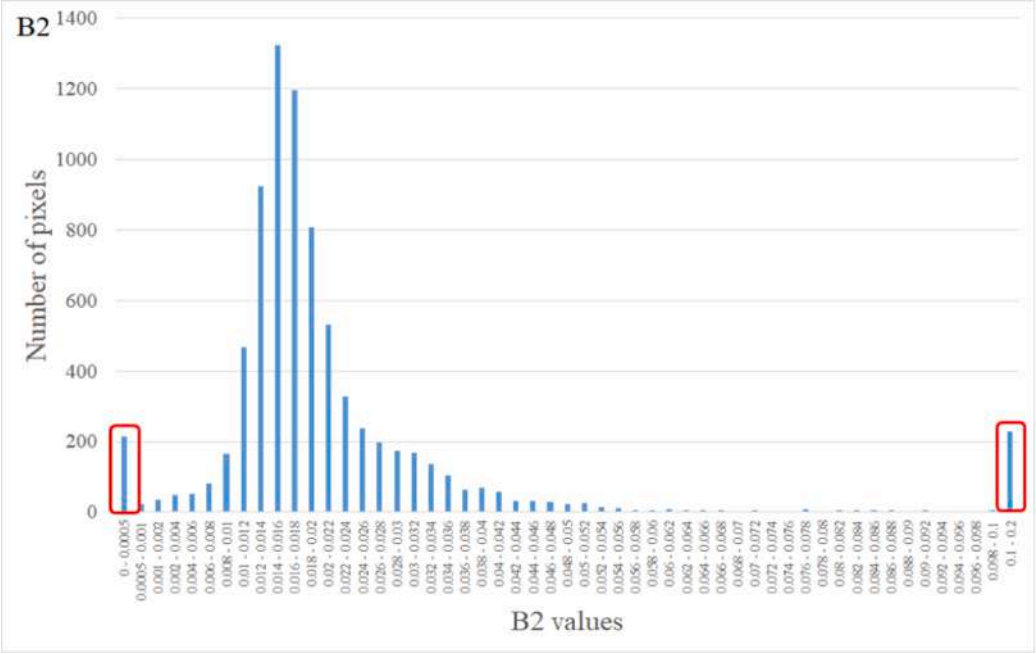

Basic Statistics B2	
N. data	8000
Mean	0.0253
Variance	0.0011
Minimum	0.0001
Maximum	0.2452

Fig. 2. Histogram and statistical parameters of Band 2 values.

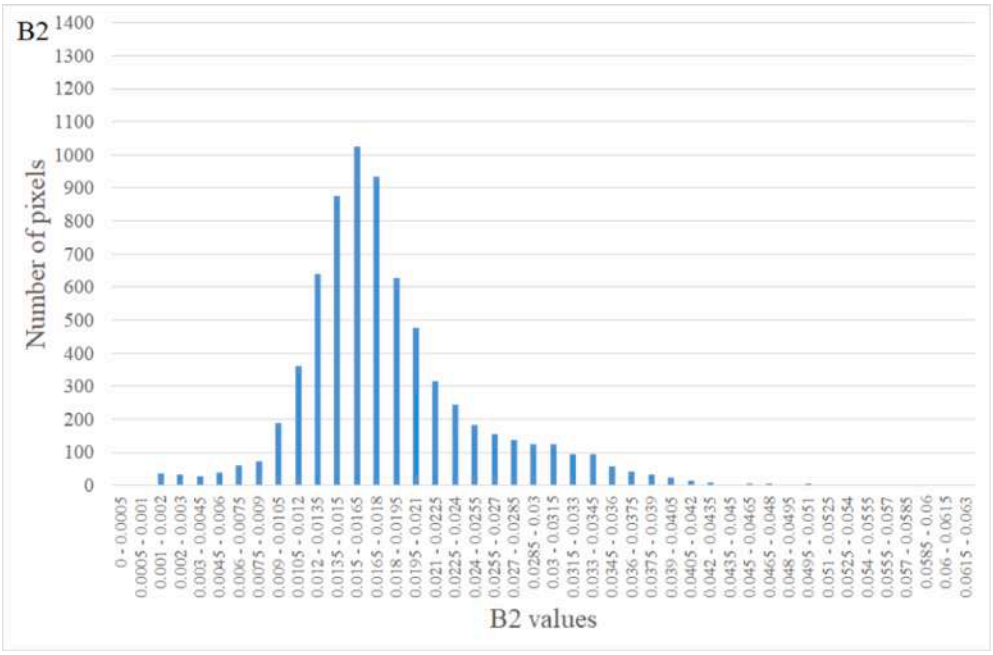

Basic Statistics B2	
N. data	6962
Mean	0.017923
Variance	0.000044
Minimum	0.001
Maximum	0.0536

Fig. 3. Histogram and statistical parameters of Band 2 values after removing the cloud and the shadow.

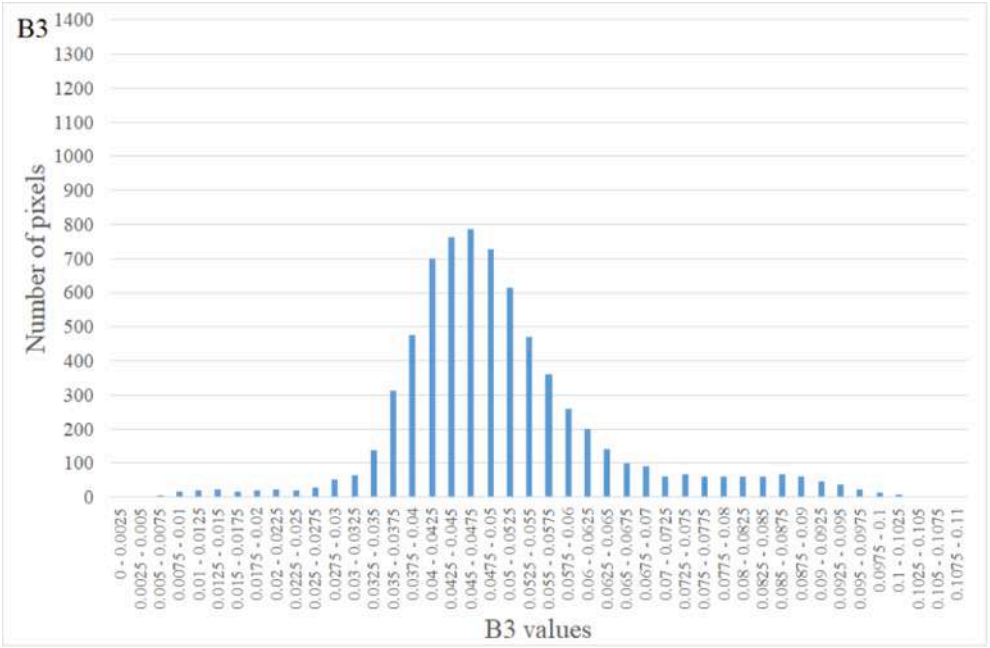

Basic Statistics B3	
N. data	6962
Mean	0.05
Variance	0.0002
Minimum	0.0021
Maximum	0.107

Fig. 4. Histogram and statistical parameters of Band 3 values after removing the cloud and the shadow.

estimation able to predict the target variable at point or block scale (Robinson et al., 2013). For both cases, the estimation result is theoretically affected by the minimum error possible, due to the minimization of the estimation variance in the Kriging algorithm (Baume et al., 2011). The variogram is the main tool for the spatial variability analysis and to optimize the Kriging estimation. The variogram indicates the influence of the samples based on the distances. Hence, the variogram of an intrinsic random function is defined as follow:

$$\gamma(h) = 0.5 \cdot Var[Z(x_i + h) - Z(x_i)] \quad (1)$$

where x_i and $x_i + h$ refer to points in an n-dimensional space (Armstrong, 1998).

The experimental variogram shows the spatial relationship between samples in space. In this application, to estimate the unknown pixels (under the cloud), it is important to analyze the spatial correlations between known pixels within the selected area. Then, the allowed mathematical variogram models can be fitted based on the spatial behavior of data (Armstrong, 1998). The experimental variograms have been calculated based on Equation (1) and are shown in the following pictures (Fig. 6). For each band value, several models were tested and the best one fitting the variogram is chosen. Furthermore, cross-validation analyses were performed to check the quality of the model for estimation (see Section 3). The best fitting model, adapted to experimental variograms of the three bands, is shown in Fig. 6 in black lines, while blue points are the calculated variogram results for various lags (Table 2).

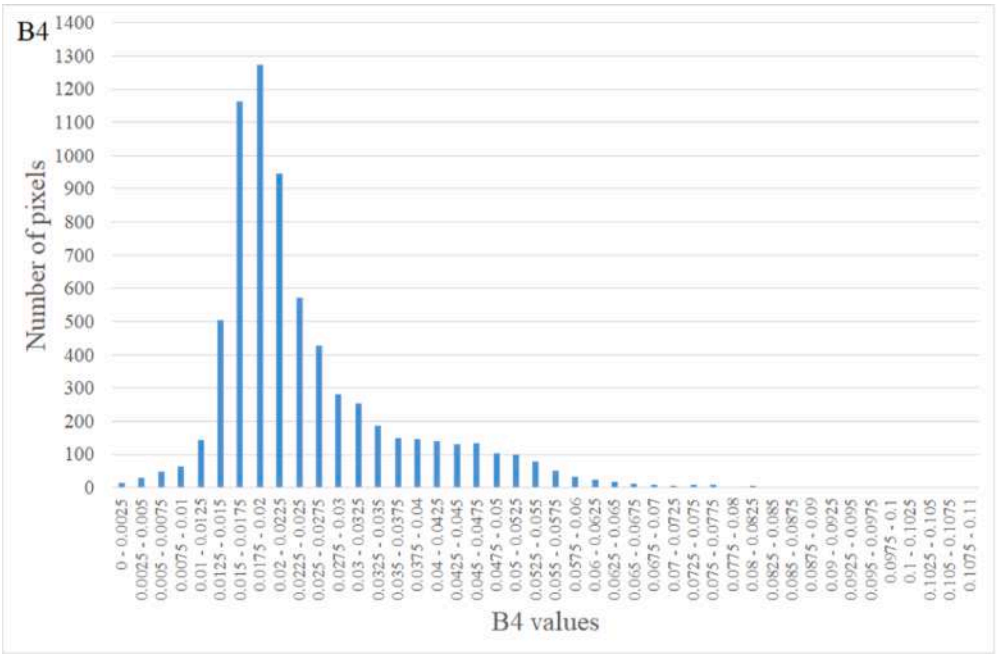

Basic Statistics B4	
N. data	6960
Mean	0.02441
Variance	0.00013
Minimum	0.0005
Maximum	0.0817

Fig. 5. Histogram and statistical parameters of Band 4 values after removing the cloud and the shadow.

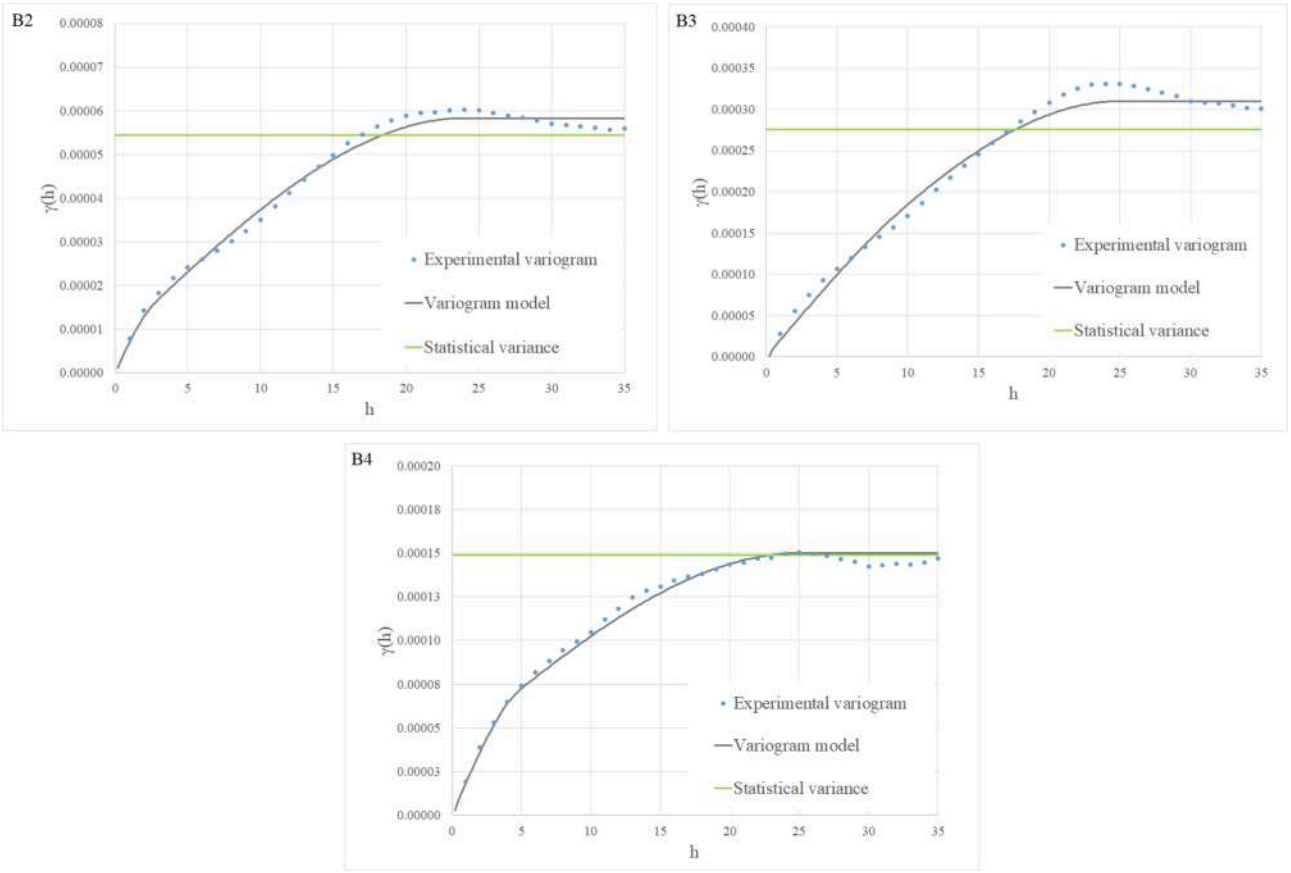

Fig. 6. Variograms of Bands 2, 3 and 4 (experimental, model and relation with the spatial variance).

The selected variogram models are presented with the chosen parameters in Table 2:

2.4. Kriging predictor

Kriging is an optimized estimation method which uses the spatial relation of data with the potential of giving the estimation variance at all

Table 2
Variogram model structures for Bands 2, 3 and 4.

Band 2 Variogram model		
Model	Spherical 1	Spherical 2
Range	23.98	2.78
Sill	0.000051	0.0000073
Band 3 Variogram model		
Model	Spherical 1	Spherical 2
Range	25	5
Sill	0.00029	0.00002
Band 4 Variogram model		
Model	Spherical 1	Spherical 2
Range	25	5
Sill	0.00011	0.00004

prediction points. The accuracy of the estimation depends on various parameters, including the number of samples, the position of the samples, the distance between the samples, and the spatial continuity of the variable (Armstrong, 1998).

Ordinary Kriging (OK: the simplest Kriging predictor) is a linear interpolator, giving the best linear estimate by minimizing the estimation variance. It also gives an unbiased estimate, since the sum of the weights equal to 1.

To estimate the target variable ($Z^*_{x_0}$) at location X_0 in the space, there is the need of samples (Z_{x_i}) at X_i locations with optimized weights:

$$Z^*_{x_0} = \sum_{i=1}^{n} (\lambda_i \bullet Z_{x_i}) \tag{2}$$

$$\sigma^{2*}_Z = Var\left(Z^*_{x_0} - Z_{x_0}\right) \tag{3}$$

Where,

$$\begin{cases} \dfrac{\partial \sigma^{2*}_Z}{\partial \lambda_i} = 0 \qquad \forall i = 1, n \\ \sum_1^n \lambda_i = 1 \end{cases} \tag{4}$$

In this case study, 596 pixels within the cloud covered area are the target points to be estimated. For each of these pixels, the RGB values (three variables) need to be predicted. OK is the first method to be tested at each pixel location. To create the final image, the estimated grid size and resolution (10 m × 10 m) is considered equal to the original image. To obtain the most coherent results and pattern of features under the clouds, different spatial neighborhoods can be tested, varying in number and position of the samples. The standard tests are about to check the Kriging estimation variance σ^{2*}_Z in all points and overall the mean and the variance of the standardized error,m_ε, σ^2_ε, according to the next equations:

$$\varepsilon = \left(Z^*_i - Z_i\right) / \sigma^*_Z \tag{5}$$

$$m_\varepsilon = E[\varepsilon] = \left(\sum_1^n \varepsilon_i\right) \Big/ n \to 0 \tag{6}$$

$$\sigma^2_\varepsilon = Var(\varepsilon) = \left(\sum_1^n \varepsilon_i^2\right) \Big/ n - m^2_\varepsilon \to 1 \tag{7}$$

where:
Z^*_i is the estimated value (for each band), while Z_i is the value of the

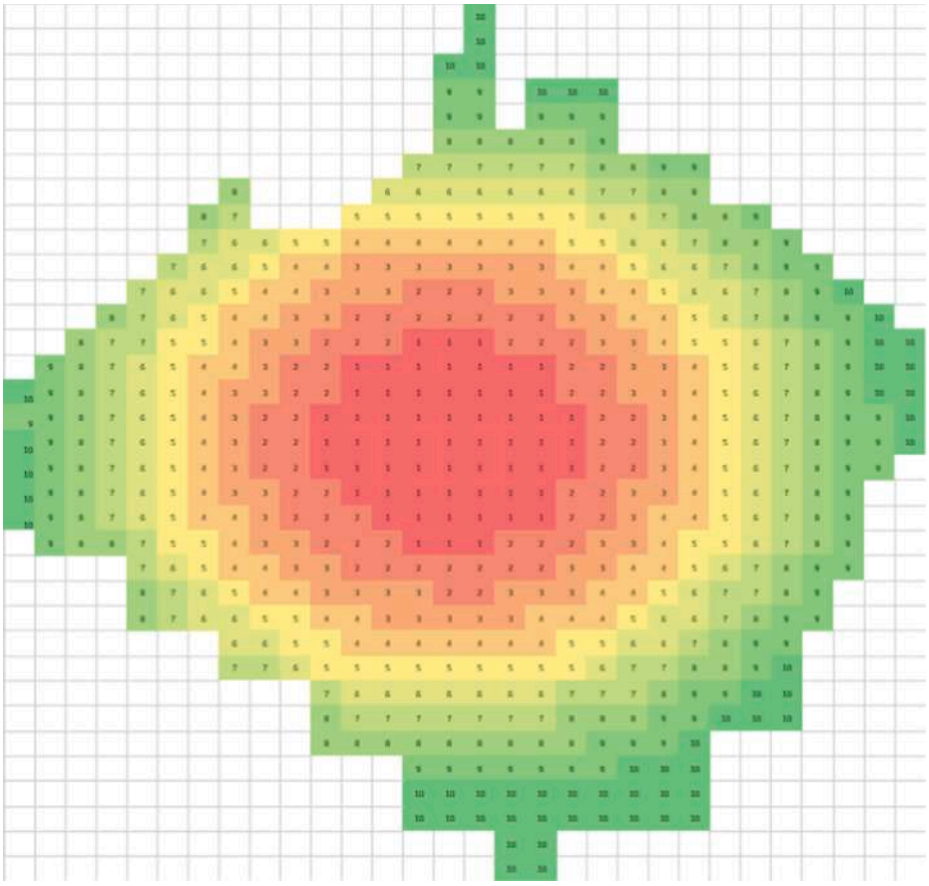

Fig. 7. Repetitive neighborhood and the pattern of selecting samples to estimate empty pixels.

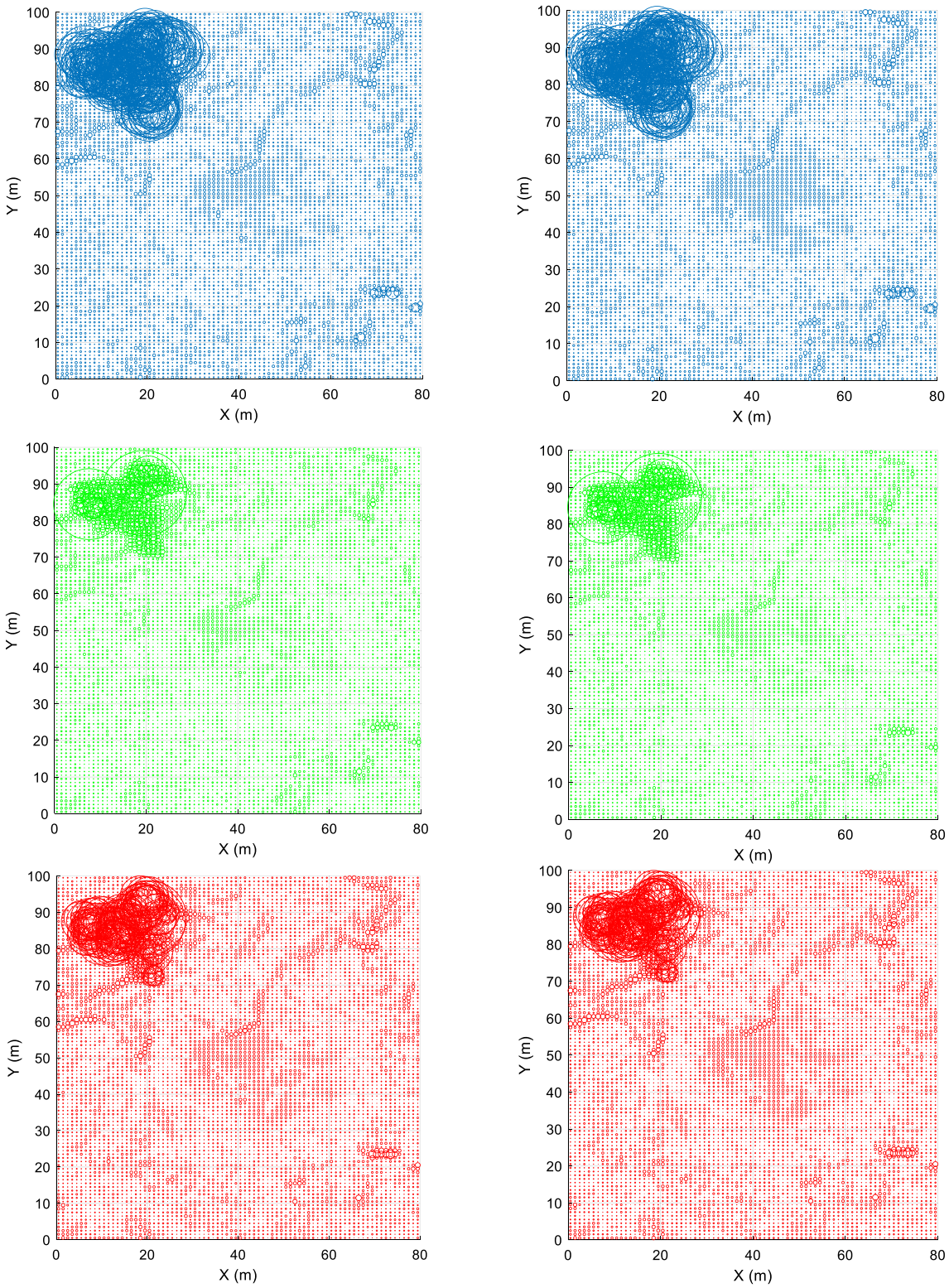

Fig. 8. Output of the MATLAB® program for unique (Right) and 4 closest pixels neighborhood (Left). The size of the circles indicates the difference in estimation value and comparison image for the three bands (blue, green and red). (For interpretation of the references to color in this figure legend, the reader is referred to the web version of this article.)

correspondent pixel in the original image. Finally, σ_Z^* is the estimation standard deviation in all points.

The nine neighborhoods considered in this work are as follows:

1. Unique neighborhood including all available samples (2006 samples) around the cloud-covered area;
2. The closest 4 samples (4 surrounded pixels) to estimate one pixel under the clouds;

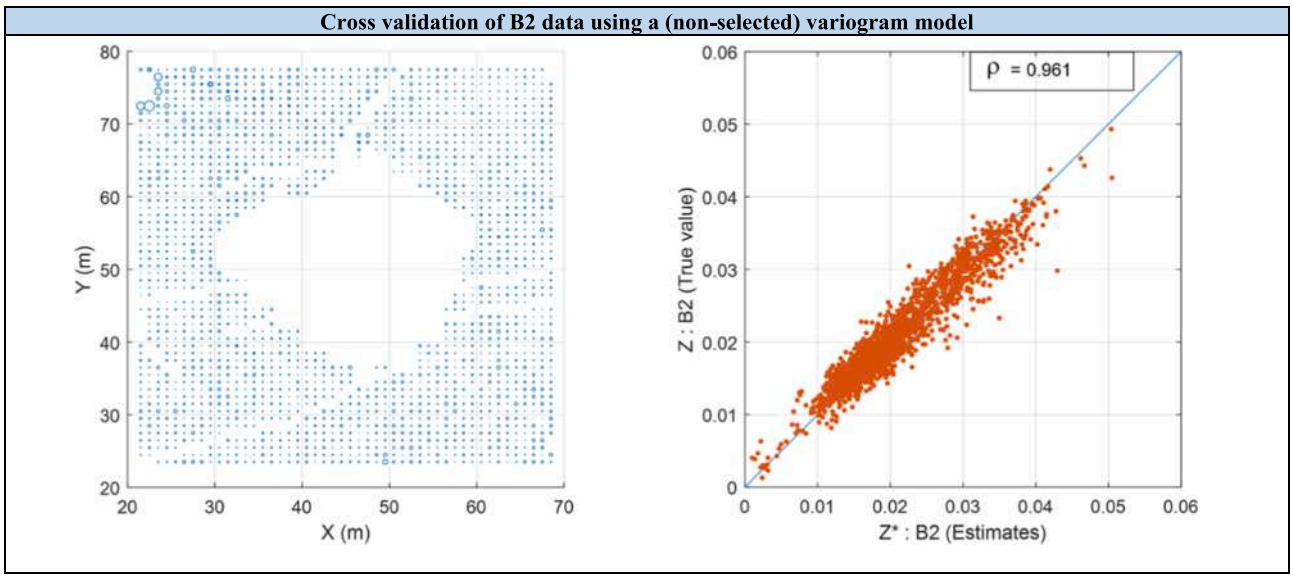

Fig. 9. Cross validation over Band 2 data: mapping the errors, where the size of each pixel indicates the estimation error points (Left); scatter plot of the estimated and real values (Right). Results obtained from a (non-selected) variogram model.

3. The closest 8 samples (8 surrounded pixels) to estimate one pixel under the clouds;
4. The closest 12 samples (12 surrounded pixels) to estimate one pixel under the clouds;
5. The closest 4 directional samples (4 closest pixels from 4 directions: 0, 90, 180 and 270) to estimate one pixel under the clouds;
6. The closest 8 directional samples (8 closest pixels from 4 directions: 0, 90, 180 and 270) to estimate one pixel under the clouds;
7. The closest 12 directional samples (8 closest pixels from 4 directions: 0, 90, 180 and 270) to estimate one pixel under the clouds;
8. Repetitive neighborhood: in this method, first, the pixels near the edge are estimated (the green pixels, starting from numbering 10). Consequently, as it is shown in Fig. 7, the estimated values on the edge (for example all pixels with number 10) of the image have been used to estimate the pixels (for example for all pixels with number 9) in the central part of the cloudy area (from green towards the red color scale, so from pixels with number 10 to those with number 1, respectively). The sequence of numbers (with specific color) shows the sequence of samples selected for estimating the following target areas.
9. Corresponding neighborhood: The simulation method has been used to fill the under-cloud area thanks to the secondary image (an image without cloud at the same location). In this method, within a secondary image (without cloud), the similar pixel values (the most similar pixels from outside of the cloud-cover area to the cloud-covered pixels) are selected as reference pixels. The same reference pixels in the image with missing values (covered by cloud) are selected and inserted to replace the cloud-covered pixels.

In order to evaluate the Kriging estimation, and to find the best variogram model, cross validation has been applied. Cross validation is a method in which known pixels (with real value) are excluded partly, or one by one, from the input, and, by using the variogram model, the removed points are estimated by the remaining data. Finally, the estimated and the real values are compared and the estimation error (simple and standardized) can be obtained (Chilès and Delfiner, 1999).

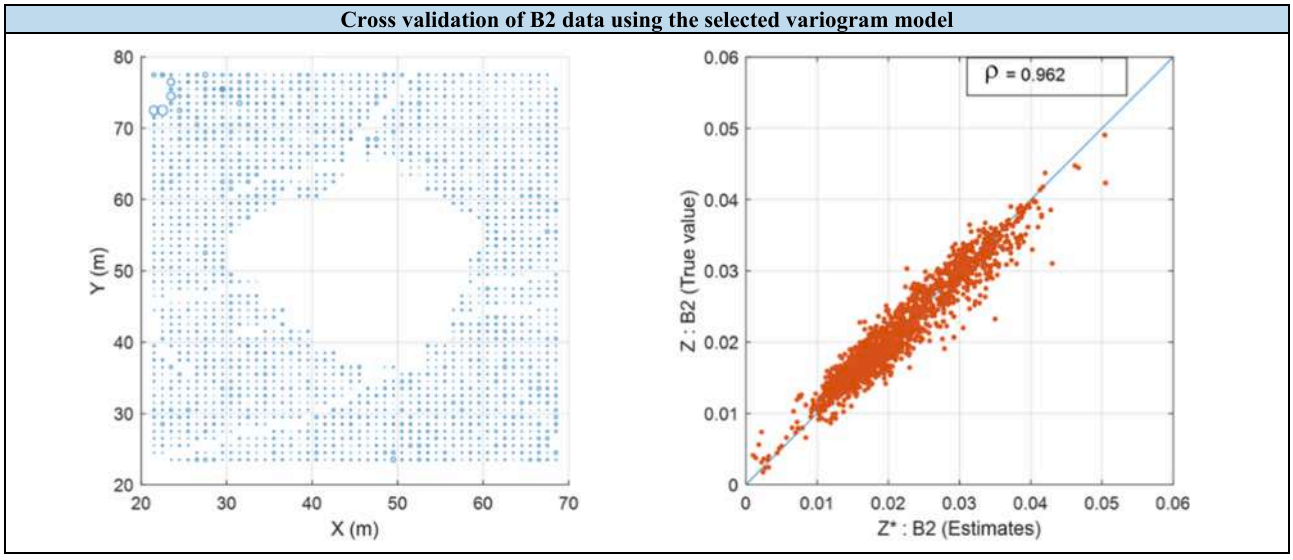

Fig. 10. Cross-validation over Band 2 data: mapping the errors, where the size of each pixel indicates the estimation error points (Left); scatter plot of the estimated and real values (Right). Results obtained from the selected variogram model.

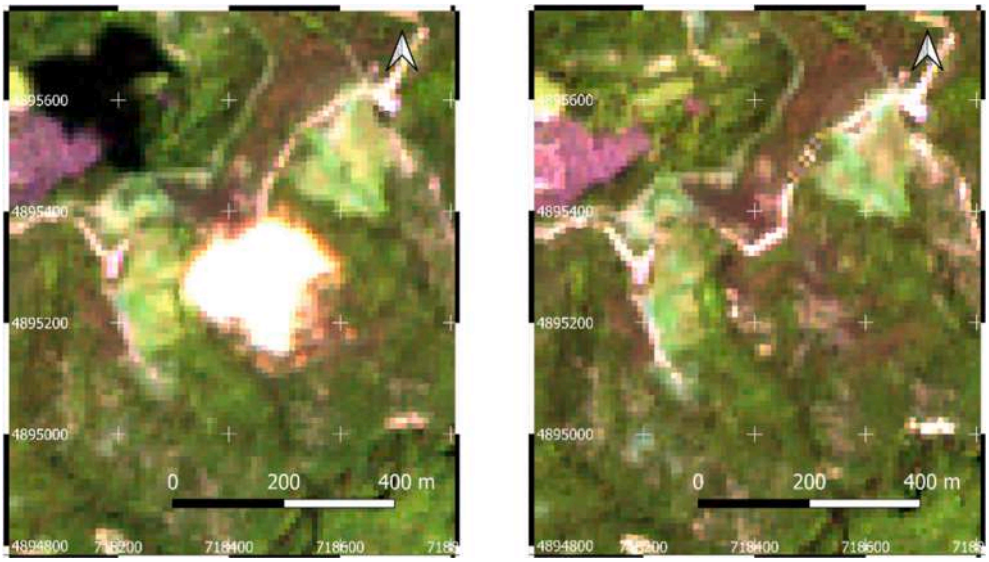

Fig. 11. The original RGB image (sensing: 2019/06/23-left) and the RGB image in closest time to the original image in real color (sensing: 2019/06/18-right).

For the selected case study and all the three variables (RGB bands), several variogram models were tested and the best result has been considered for the estimation.

For the project, the OK method has been implemented using MATLAB® programming. The Kriging calculations (inversion of the variogram matrix and other matrix operations) have been implemented. The created program also allows to import the samples, with their locations, and the coordinates of the unknown pixels from the various datasets and images, too, by the aid of a second program, called "Import". The OK function has been applied to each target pixel, using the given neighborhood among the nine possibilities presented above. Finally, the developed program allows to visualize the estimation results in form of a 2D scatterplot, with circles, proportional to the difference of estimated values with respect to the ones of a comparative image. For the specific challenge of under-cloud RGB estimation, the size of each point indicates the deviation of the band value between the original image (with the cloud) and a second image (without the cloud).

3. Results

The three main band values (RGB) have been estimated, using the nine neighborhoods described in Section 2. To prepare the RGB images from results, the estimated bands were imported into QGIS and transformed into raster outputs (all outputs with 10 m × 10 m pixel size), through "rasterize" command. The coordinate system of results is WGS84-UTM Zone 32 N. Then, the RGB images have been obtained through QGIS algorithm of nearest neighborhood interpolation. The obtained raster images from OK estimation have been compared with an image with closest sensing date (sensing: 2019/06/18) to the original one (sensing: 2019/06/23). The estimation results for two different neighborhoods, the unique neighborhood and the 4 closest pixels, are presented in the scatter plots of Fig. 8. In order to evaluate the results, estimated values are compared to the band values of the image with closest sensing date.

The difference between the estimated band values and the ones of the comparison image has been calculated for each pixel. On the upper left corner, where there is a shadow, the differences are dramatically high, so the circles have very large size. However, in the center of the image, with the target under-cloud zone, the differences reduce. Before estimation, the consistency of the variogram models were checked. The following figures, specific for the B2 values, display the map of error and the scatter plot of the cross validation, obtained using two different variogram models and considering a unique neighborhood for all estimations. Spearman correlation coefficient ρ has been calculated for estimates and true values, in order to compare the different models quantitatively.

For all bands, the same procedures have been performed and the most coherent variogram model has been chosen for the estimation. The original image (Fig. 11) including the cloud and the shadow is shown with the image (with closest time) without cloud. These two images are considered as the reference images, the first one for estimation of the under-cloud pixels and the second one for validation of the final results. Several neighborhoods have been considered to check the best consistency of results.

The obtained results using the various neighborhoods are presented in Fig. 12.

In Table 3, the statistical indicators, mean and standard deviation over the standardized error calculated in all pixels, are presented for the three bands 2, 3 and 4, for all the estimation techniques used. Note that the range of pixel values are 0 to 255. It is worth saying that for the corresponding neighborhood method, not using geostatistical estimation, it is not possible to calculate the estimation variance and then the standardized error (See Equation (5)). For this reason, Table 3 does not comprehend the statistical indicators of the corresponding neighborhood method, since this method has no possibility to calculate the estimation variance and then the standardized error.

In order to include the corresponding neighborhood method in the comparison of results, the mean and estimation variance of the simple absolute error $\varepsilon_{abs} = \left|Z_i^* - Z_i\right|$ have been calculated. The results are reported in Table 4.

4. Discussion

As evidenced in Fig. 9 and Fig. 10 (as example for Band 2), cross-validation results have shown a relevant correlation, obtained between the estimated values and real ones using the defined fitted variogram models ($\rho = 0.96$) As it is shown in Fig. 12, for each selected neighborhood, through the estimation different results have been obtained in terms of deviation from the comparison image. First of all, using neighborhoods with few closest pixels, the estimation can be affected by samples only from one side of the area. The reason is that in this case only the distance is the main factor for choosing the surrounded samples for estimation. However, in directional neighborhoods (e.g. 4-directional samples), the target area has been divided into 4 sections (based on 0, 90, 180 and 270°) and from each section, one pixel has been taken for estimation (4 pixels in total). The same logic has been used for

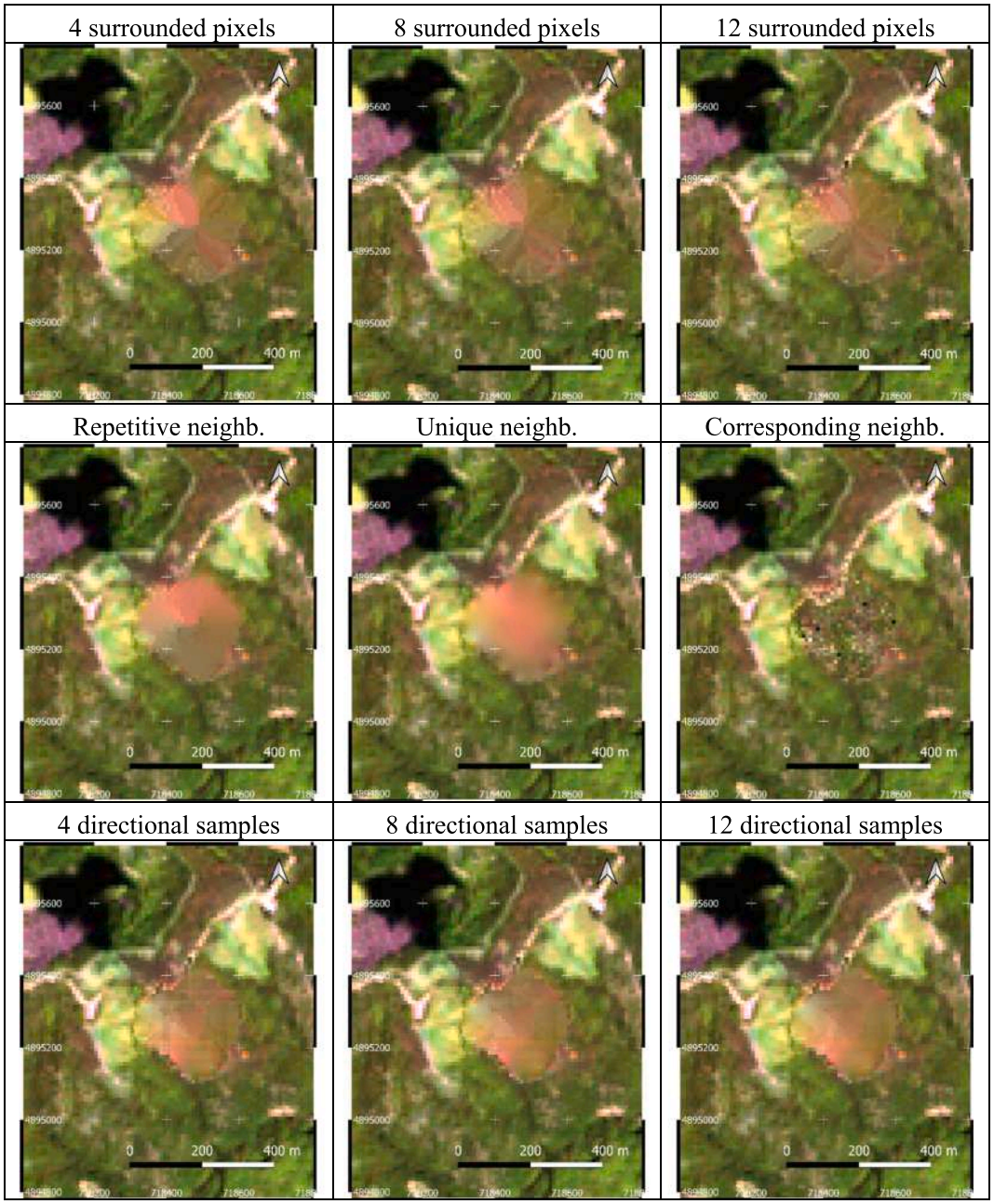

Fig. 12. RGB estimation results using the various possible neighborhoods.

Table 3
Values of statistical indicators (mean and standard deviation) over the standardized error for the three bands and for the various estimation methods used.

Neighborhood		Statistical indicators over the standardized error for the three bands					
		B2		B3		B4	
		Mean	Standard deviation	Mean	Standard deviation	Mean	Standard deviation
1	Unique neighb.	−1.76	2.71	−0.83	1.85	−0.85	2.21
2	Closest 4 pixels	−0.45	1.03	−0.27	0.68	−0.23	0.94
3	Closest 8 pixels	−0.37	1.08	−0.24	0.70	−0.18	0.98
4	Closest 12 pixels	−0.31	1.13	−0.22	0.75	−0.14	1.04
5	Directional 4 pixels	−1.12	2.55	−0.70	1.55	−0.47	1.69
6	Directional 8 pixels	−1.17	2.57	−0.72	1.57	−0.50	1.71
7	Directional 12 pixels	−1.27	2.62	−0.76	1.58	−0.55	1.74
8	Repetitive neighb.	−0.59	1.10	−0.24	0.63	−0.40	1.02

Table 4
Values of statistical indicators (mean and standard deviation) over the simple absolute error for the three bands and for the various estimation methods used.

Neighborhood		Statistical indicators over the simple error for the three bands					
		B2		B3		B4	
		Mean	Standard deviation	Mean	Standard deviation	Mean	Standard deviation
1	Unique neighb.	0.00756	0.01177	0.01086	0.01315	0.01043	0.01310
2	Closest 4 pixels	0.00791	0.00853	0.01189	0.01255	0.01088	0.01159
3	Closest 8 pixels	0.00814	0.00811	0.01186	0.01239	0.01131	0.01124
4	Closest 12 pixels	0.00835	0.00793	0.01661	0.01239	0.01180	0.01120
5	Directional 4 pixels	0.00846	0.00954	0.01195	0.01273	0.01221	0.01331
6	Directional 8 pixels	0.00831	0.00955	0.01174	0.01270	0.01195	0.01334
7	Directional 12 pixels	0.00835	0.00988	0.01170	0.01293	0.01191	0.01350
8	Repetitive neighb.	0.00813	0.01006	0.01073	0.01210	0.01126	0.01421
9	Corresponding neighb.	0.00729	0.00441	0.00743	0.00562	0.00920	0.00528

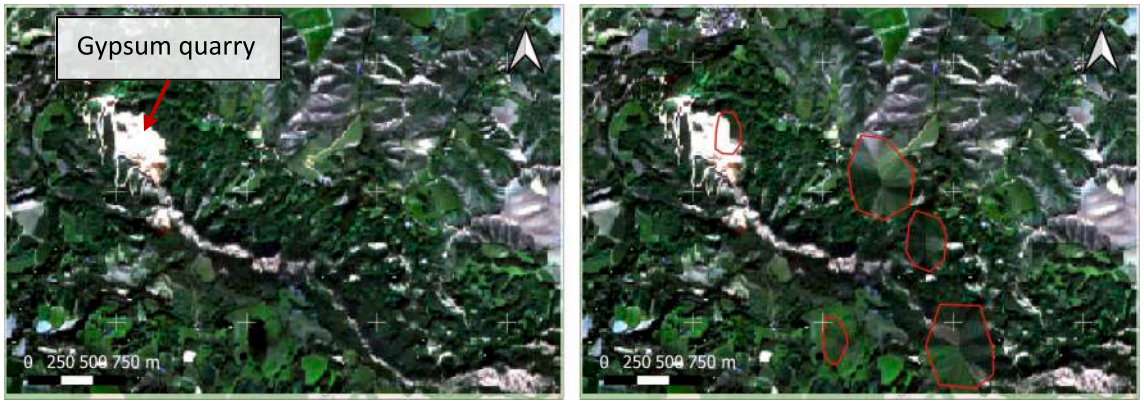

Fig. 13. The RGB image of a gypsum quarry (Left) and the OK estimation results using 12 closest pixel-neighborhood (Right). The red polygons show the boundaries of the shadow and the clouds. (For interpretation of the references to color in this figure legend, the reader is referred to the web version of this article.)

8 and 12-directional samples. Results have been improved by applying directional sampling, since surrounded areas from 4 sides were considered. Finally, the unique neighborhood shows the less-patterned results, because of using all pixel-values in the image (affected by distances and their weights). Although the directional neighborhood could solve the smoothing effect of Kriging estimated results, however, the results remain still less precise, since they are related to the central part of the under-cloud pixels. Farther the empty pixels are from the available samples, the less precise and more smoothed are the estimation results. Using a corresponding neighborhood have showed similar results to random selection of samples. Although samples were selected by the closest pixel-values, however, no spatial correlation and structure have been considered for filling the empty pixels. In this method, the pattern of results is closer to the reality, but with high outliers in the results. Moreover, in this method, always there is the need of finding a closely image without clouds. Hence, the challenge of finding subsequent images (which are usually still with cloud cover) of the target area remains. From a statistical point of view, Table 3 and Table 4 show the standard deviation and the mean of, respectively, the standardized and simple absolute errors, which were obtained from comparison of the two images of Fig. 11. Results evidenced how the closest 12 pixels method presents the best performance, approaching the optimum theoretical result (mean → 0, standard deviation → 1). In any case, many geostatistical estimation methods have good performances, however the corresponding neighborhood, which means using a second image as a benchmark to estimate the first image, has always better performance (as it may be expected). In absence of a second image, the geostatistical estimation method proved to be robust, theoretically and practically. It

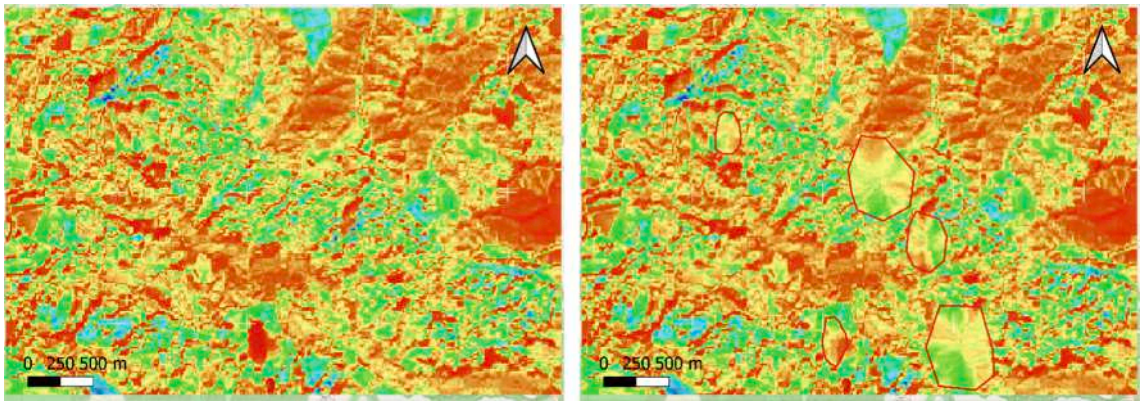

Fig. 14. The NIR band false-colored image (Left) and the OK estimation results using 12 closest pixel-neighborhood (Right). The red polygons show the boundaries of the shadow and the clouds. (For interpretation of the references to color in this figure legend, the reader is referred to the web version of this article.)

is important to remark that, despite the similarity, some physical-technical differences (because of light) between the original image (the image with cloud, sensing 2019/06/23) and the close-time image (as the reference image, sensing 2019/06/18) remain.

The approach is used to estimate RGB bands to create the final RGB images (real-colored images). Additionally, the approach has been tested also for the Near Infrared band (NIR). Hence, it can be performed for all the remained bands (e.g. Short-Wave Infrared, etc.). Moreover, it can be used for larger images with more complex cloud cover. As an example, the geostatistical approach has been repeated over a highly disturbed image, in the same area of the gypsum quarry case study as shown in Fig. 13. In this image the OK with the closest 12 pixels neighborhood is performed to create the features where needed (under one shadow and four clouds in various location of the image). The shadow and clouds locations are defined with red-polygons in Fig. 13. The result of the tested approach for the NIR bands on the same case study is shown in Fig. 14.

Based on the obtained results, as an advantage, the size of the image seems not affecting the quality of the approach. The reason is that the OK estimation is obtained by the pixels closest to the target clouds or shadows. Therefore, it is suggested to cut the image, and work on smaller subsets to require less computational ability. However, the main challenging point is the definition of the clouds' boundaries and the removal of all bright (as clouds) and black (as shadows) pixels. In fact, any remained noisy pixel around the cloud can affect the estimation results, by re-creating hazy areas. Hence, the proposed method is challenging for thin or hazy clouds. Moreover, the smaller the cloud is, the better this method can predict. In fact, with large clouds, the error increases because of the smooth effect of OK, and therefore this method can hardly predict alone the complex patters under large clouds.

5. Conclusions

The estimation of under-cloud pixels is a big challenge in remote sensing. In this research work, the numerical estimation approaches have been tested for the first time. The geostatistical estimation method of OK has been used with various types of neighborhoods to evaluate the possibility of predicting the pixel values under clouds. The spatial variability of three main bands (RGB) has been studied to gain the best possible variogram models, fitted on experimental variograms. Hence, the spatial behavior of data has been analyzed around the area covered by the cloud. Various estimation neighborhoods have been tested and the results have been compared. The obtained raster images from estimations have demonstrated (even though with some limitations) the possible prediction of pixel values under the cloud area. The geostatistical OK tool, combined with GIS pre and post-processing of the images, can be successfully applied for the scope. The main advantages of using geostatistical tools are:

- Considering the spatial correlation and spatial variability of pixel values within the variogram analysis;
- Providing a fast and robust prediction method based on the obtained spatial structure of data;
- Giving the possibility of testing various parameters while filling the missing pixel values and the possibility of changing the smoothing effects on the image;
- Obtaining the uncertainty for each pixel prediction, which demonstrates the estimation precision.

The main limitation of this approach, however, resides in the difficulties of predicting the distinctive features under the clouds. Since the approach is based on the continuous spatial variability, in the case of some peak values under the clouds, the results might be still smoothed. This point should be considered for the future research, for example through the application of indicators (related to the features classifications) or by adding extra parameters to improve the estimations using multivariate geostatistical approaches.

CRediT authorship contribution statement

A. Tayebi: Conceptualization, Methodology, Investigation, Data curation, Validation, Formal analysis, Writing – original draft, Writing – review & editing. **S. Kasmaeeyazdi:** Investigation, Data curation, Validation, Formal analysis, Writing – original draft, Writing – review & editing. **F. Tinti:** Validation, Formal analysis, Writing – original draft, Writing – review & editing, Project administration. **R. Bruno:** Conceptualization, Methodology, Validation, Formal analysis, Supervision, Writing – original draft.

Declaration of Competing Interest

The authors declare that they have no known competing financial interests or personal relationships that could have appeared to influence the work reported in this paper.

Data availability

Data will be made available on request.

Funding

This work was supported by the RawMatCop Alliance Project (2022-2024), funded by EIT RawMaterial, Project Agreement number 21118 under Horizon Europe Partnership Agreement PA2021/EIT/EIT.

Appendix A. Supplementary data

Supplementary data to this article can be found online at https://doi.org/10.1016/j.jag.2023.103236.

References

Armstrong, M. (1998). Basic Linear Geostatistics. Heidelberg: Springer Berlin, Heidelberg. doi: https://doi.org/10.1007/978-3-642-58727-6.

Baume, O., Skoien, J., Heuvelink, G., Pebesma, E., Melles, S., 2011. A geostatistical approach to data harmonization – Application to radioactivity. Int. J. Appl. Earth Observation 13, 409–419. https://doi.org/10.1016/j.jag.2010.09.002.

Cheng, Q., Shen, H., Zhang, L., Yuan, Q., Zeng, C., 2014. Cloud removal for remotely sensed images by similar pixel replacement guided with a spatio-temporal MRF model. ISPRS J. Photogramm. Remote Sens. 92, 54–68. https://doi.org/10.1016/j.isprsjprs.2014.02.015.

Chilès, J., Delfiner, P., 1999. Geostatistics: Modeling Spatial Uncertainty. Wiley, New York. https://doi.org/10.1002/9780470316993.

Helmer, E., Ruefenacht, B., 2005. Cloud-Free Satellite Image Mosaics with Regression Trees and Histogram Matching. Photogramm. Eng. Remote Sens. 1079–1089 https://doi.org/10.14358/PERS.71.9.1079.

Ibrahim, E., Lema, L., Barnabé, P., Lacroix, P., Pirard, E., 2020. Small-scale surface mining of gold placers: Detection, mapping, and temporal analysis through the use of free satellite imagery. Int. J. Appl. Earth Obs. Geoinf. 93, 102194 https://doi.org/10.1016/j.jag.2020.102194.

Jiang, B., Li, X., Chong, H., Wu, Y., Li, Y., Jia, J., Wang, S., Wang, J., Chen, X., 2022. A deep-learning reconstruction method for remote sensing images with large thick cloud cover. Int. J. Appl. Earth Observat. Geoinformat. 115, 103079 https://doi.org/10.1016/j.jag.2022.103079.

Kasmaeeyazdi, S., Mandanici, E., Balomenos, E., Tinti, F., Bonduà, S., Bruno, R., 2021. Mapping of Aluminum Concentration in Bauxite Mining Residues Using Sentinel-2 Imagery. Remote Sens. (Basel) 13, 1517. https://doi.org/10.3390/rs130815.

Kayet, N., Pathak, K., Singh, C., Chowdary, V., Bhattacharya, B., Kumar, D., Shaik, I., 2022. Vegetation health conditions assessment and mapping using AVIRIS-NG hyperspectral and field spectroscopy data for -environmental impact assessment in coal mining sites. Ecotoxicol. Environ. Saf. 239 https://doi.org/10.1016/j.ecoenv.2022.113650.

Li, X., Ling, F., Cai, X., Ge, Y., Li, X., Yin, Z., Shang, C., Jia, X., Du, Y., 2021. Mapping water bodies under cloud cover using remotely sensed optical images and a spatiotemporal dependence model. Int. J. Appl. Earth Observat. Geoinformat. 103, 102470 https://doi.org/10.1016/j.jag.2021.102470.

Lorenzi, L., Melgani, F., Mercier, G., 2011. Inpainting Strategies for Reconstruction of Missing Data in VHR Images. IEEE Geosci. Remote Sens. Lett. 8 (5), 914–918. https://doi.org/10.1109/LGRS.2011.2141112.

Maalouf, A., Carre, P., Augereau, B., Fernandez, C., 2009. A Bandelet-Based Inpainting Technique for Clouds Removal From Remotely Sensed Images. 47 (7) https://doi.org/10.1109/TGRS.2008.2010454.

Matheron, G. (1971). The Theory of Regionalized Variables and Its Application. Paris: Ecole Nationale Supérieure des Mines de Paris.

Melgani, F., 2006. Contextual reconstruction of cloud-contaminated multitemporal multispectral images. IEEE Trans. Geosci. Remote Sens. 44 (2), 442–455. https://doi.org/10.1109/TGRS.2005.861929.

Meng, Q., Borders, B.E., Cieszewski, C.J., Madden, M., 2009. Closest Spectral Fit for Removing Clouds and Cloud Shadows. Photogramm. Eng. Remote Sens. 569–576 https://doi.org/10.14358/PERS.75.5.569.

Meng, F., Yang, X., Zhou, C., Li, Z., 2017. A Sparse Dictionary Learning-Based Adaptive Patch Inpainting Method for Thick Clouds Removal from High-Spatial Resolution Remote Sensing Imagery. Sensors 17 (9). https://doi.org/10.3390/s17092130.

Ngom, N.M., Mbaye, M., Baratoux, D., Baratoux, L., Ahoussi, K.E., Kouame, J.K., Faye, G., Sow, E.H., 2022. Recent expansion of artisanal gold mining along the Bandama River (Cote d'Ivoire). Int. J. Appl. Earth Observat. Geoinformat. 112, 102873 https://doi.org/10.1016/j.jag.2022.102873.

Pascucci, S., Belviso, C., Caval, R.M., 2012. Using imaging spectroscopy to map red mud dust waste: The Podgorica Aluminum Complex case study. 123, 139–154. https://doi.org/10.1016/j.rse.2012.03.017.

Patino, J., Duque, J., 2013. A review of regional science applications of satellite remote sensing in urban settings. Comput. Environ. Urban Syst. 1–17 https://doi.org/10.1016/j.compenvurbsys.2012.06.003.

Robinson, D., Lloyd, C., McKinley, J., 2013. Increasing the accuracy of nitrogen dioxide (NO2) pollution mapping using geographically weighted regression (GWR) and geostatistics. Int. J. Appl. Earth Obs. Geoinf. 21 (1), 374–383. https://doi.org/10.1016/j.jag.2011.11.001.

Rohden Prudente, V., Martins, V., Corte Vieira, D., de França e Silva, N., Adami, M., Del'Arco Sanches, I. (2020). Limitations of cloud cover for optical remote sensing of agricultural areas across South America. Remote Sensing Applications: Society and Environment, 20, 100414. doi: https://doi.org/10.1016/j.rsase.2020.100414.

Shrestha, D.P., Saepuloh, A., Van der Meer, F., 2019. Land cover classification in the tropics, solving the problem of cloud covered areas using topographic parameters. Int. J. Appl. Earth Observat. Geoinformat. 88, 84–93. https://doi.org/10.1016/j.jag.2018.12.010.

Swayze, G., Smith, K., Clarck, R., Sutley, S., 2000. Using imaging spectroscopy to map acidic mine waste. Environ. Sci. Tech. 34 (1), 47–54. https://doi.org/10.1021/es990046w.

The European Space Agency. (2022, 10 25). *Sentinel-2*. Retrieved from ESA: https://www.esa.int/.

Van der Meer, F., Hecker, C., Van Ruitenbeek, F., Van der Werff, H., De Wijkerslooth, C., Wechsler, C., 2014. Geologic remote sensing for geothermal exploration: A review. Int. J. Appl. Earth Observat. Geoinformat. 33, 255–269. https://doi.org/10.1016/j.jag.2014.05.007.

Wang, R.Q., 2022. A recommender system-inspired cloud data filling scheme for satellite-based coastal land use classification. Int. J. Appl. Earth Obs. Geoinf. 109 https://doi.org/10.1016/j.jag.2022.102770.

Wang, L., Wang, Q., 2022. Fast spatial-spectral random forests for thick cloud removal of hyperspectral images. Int. J. Appl. Earth Obs. Geoinf. 112 https://doi.org/10.1016/j.jag.2022.102916.

Xu, Z., Sun, J., 2010. Image inpainting by patch propagation using patch sparsity. IEEE Trans Image Process 19. https://doi.org/10.1109/TIP.2010.2042098.

Zhu, X., Gao, F., Liu, D., Chen, J., 2012. A Modified Neighborhood Similar Pixel Interpolator Approach for Removing Thick Clouds in Landsat Images. IEEE Geosci. Remote Sens. Lett. 9, 521–525. https://doi.org/10.1109/LGRS.2011.2173290.